KSME

Springer

Journal of Mechanical Science and Technology 37 (8) 2023

Original Article
DOI 10.1007/s12206-023-0737-6

Keywords:
· Structural health monitoring
· Guided wave
· Lamb wave
· Incident angel crack
· Finite element method
· Piezoelectric sensor
· Simulation

Correspondence to:
Sanghoon Lee
shlee1222@kmu.ac.kr

Citation:
Kim, S., Kim, N. H., Lee, S. (2023). Study on Lamb wave propagation in a cracked plate using numerical simulations. Journal of Mechanical Science and Technology 37 (8) (2023) 4217~4225.
http://doi.org/10.1007/s12206-023-0737-6

Received February 14th, 2023
Revised March 20th, 2023
Accepted April 6th, 2023

† Recommended by Editor
Hyun-Gyu Kim

© The Korean Society of Mechanical Engineers and Springer-Verlag GmbH Germany, part of Springer Nature 2023

Study on Lamb wave propagation in a cracked plate using numerical simulations

Seyeon Kim[1], Nam H. Kim[2] and Sanghoon Lee[1]

[1]Department of Mechanical Engineering, Keimyung University, Daegu 42601, Korea, [2] Department of Mechanical and Aerospace Engineering, University of Florida, Gainesville, FL 32611, USA

Abstract Most cracks do not grow straight due to the inhomogeneity of material properties. Furthermore, quantifying structural damage using Lamb waves is difficult due to uncertain crack shape. Here, we present a newly developed finite element model to simulate the propagation of Lamb waves in a cracked plate to quantify the influence of crack size and orientation on the characteristics of Lamb wave propagation. This model includes a piezoelectric actuator and sensor to generate and receive the tone-burst signals of Lamb wave. The damping coefficient of the finite element model was calibrated with the experimental data of plates without a crack. The Lamb wave propagation simulations were performed with various crack sizes, crack orientations, and distances between the actuator and sensor. Our model was utilized to investigate the influence of crack orientation on damage quantification based on the signal phase change and normalized amplitude. We successfully evaluated the effect of the incident angle of the crack, crack size, and distance between the sensors on the change of the plate wave signal characteristics. The signal characteristics obtained from our novel finite element model can be used to develop a quantification model to estimate the crack size, direction, and distance from the sensor.

1. Introduction

Structural systems in various applications degrade over time, eventually becoming damaged to a degree that threatens the safety of the structure. To prevent catastrophic structural failure, it is crucial to develop structural health monitoring (SHM) technology that can pre-emptively detect damage and estimate its severity. Guided waves are commonly used in the industry as a tool for SHM, which can detect and estimate damage in a structure [1-4]. Lamb waves are guided waves that can be classified into two vibrations modes: S-mode and A-mode. They are useful for SHM as they can travel a long distance without losing energy [1]. Most research uses the decay coefficient of Lamb waves to estimate the level of damage in a structure [5-9]. Chang et al. used PZT actuators to generate Lamb waves and to receive signals. They developed various diagnostics technologies and proved the effectiveness of their model for crack detection on the surface of metals [10, 11]. Ihn and Chang used damage index (DI) in the S_0 mode wave packet to monitor fatigue crack growth [5].

However, it is difficult to quantify damage using Lamb wave due to the uncertain shape of cracks. Most cracks do not grow straight due to the inhomogeneity of material properties and if the crack is idealized as a straight one it can cause errors. Crack size is directly related with the fatigue life of a structure and the orientation of a crack can significantly affect the quantification of its size [12]. In this research, finite element analyses are utilized to characterize Lamb wave propagation in the existence of cracks with various sizes and orientations. Here, we develop a simulation model which can replace physical experiments so that Lamb wave characteristics under various situations can be thoroughly investigated. The data obtained in this work can be utilized in future studies to generate a quantification model for crack size and orientation, and eventually for estimating the remaining useful life of a steel structure with cracks by combining

the crack growth model and loading history.

2. Guided wave

Guided waves are crucial for SHM to detect damage in a structure. A guided wave is an ultrasonic vibration that propagates through the length of a structure making it possible to estimate its health state by analyzing the change in amplitude, shape, and characteristics of the wave [4].

2.1 Lamb wave

The wave mode is defined as the vibration of particles during wave propagation. In a solid medium, the material is elastically displaced to generate a longitudinal wave, transverse wave, surface wave and plane wave. The Lamb wave used in this study is a plane stress wave generated in a plate with a free boundary condition. It consists of longitudinal and transverse waves passing through the thickness of the specimen and considers only the displacement through the propagation direction of the wave [13].

Horace Lamb was the first to study Lamb waves in 1917 [14]. Lamb waves propagate on a thin plate, where they generate elliptical motion by combining longitudinal and transverse motions [5]. These waves can be classified into S-mode (symmetric) and A-mode (asymmetric) based on the shape of the vibration mode. S-mode moves symmetrically with respect to the neutral axis of the plate and its motion extends and compresses the plate. A-mode moves up and down asymmetrically through the neutral axis and resembles the displacement field of the simple flexural wave. Lamb waves have a dispersion property, and their velocity and frequency depend on the thickness of the plate. The wave can propagate a long distance without losing much energy, making it useful for SHM [1].

2.2 Wave frequency selection

The speed of guided waves can be explained with phase velocity and group velocity which can distort the signal even at a specific frequency because waves with different velocities interfere with each other. Therefore, it is important to select a frequency based on the dispersion curve. Fig. 1 shows the dispersion curve of a Lamb wave in a 2 mm thick aluminum plate [14]. In our study, 160 kHz frequency is selected to limit the dispersal of the guided wave and ensure there is no interference between the S_0 and A_0 mode. In this case, the group velocity of the S_0 mode and A_0 mode is 5.33 mm/μsec and 2.26 mm/μsec, respectively.

2.3 Tone burst signal of a lamb wave

For our study, the Hanning window was applied to the Lamb wave of 160 kHz frequency. The Hanning window can limit the excitation frequency range and reduce the reflection between waves and the energy of specific frequencies. As the number

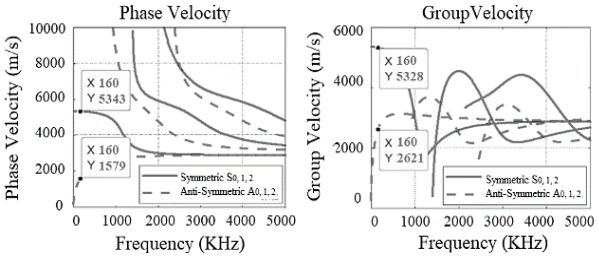

Fig. 1. Lamb wave dispersion curve in a 2 mm thick aluminum plate.

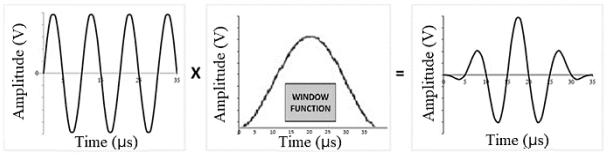

Fig. 2. 3.5-cycle tone burst signal for a Lamb wave.

of cycles in the Hanning window signal increases, the dispersion of excitation frequency is reduced; however, it requires longer tone burst signals and low resolution [4]. In general, a 5-cycle sine wave is used as a tone burst signal due to its adequate dispersion characteristics [5, 16-20]. However, the 5-cycle tone burst signal is too long for the 400 mm aluminum plate considered in this study, causing interference between the excitation signals and reflected signals; therefore, a Hanning window signal with a 3.5-cycles tone burst signal is utilized. The sine wave and the Hanning window are formulated in Eqs. (1) and (2). Using Eqs. (1) and (2), the tone burst signal $y(t)$ is formulated, as in Eq. (3) and shown in Fig. 2:

$$S(t) = A \times sinsin(2\pi f_c t) \tag{1}$$

$$W(t) = \frac{1}{2} \times \left(1 - cos\left(\frac{2\pi f_c t}{N}\right)\right) \tag{2}$$

$$y(t) = A \times sinsin(2\pi f_c t) \frac{1}{2} \times \left(1 - cos\left(\frac{2\pi f_c t}{N}\right)\right) \tag{3}$$

where A denotes the maximum amplitude, f_c is the center frequency, t is the total signal time, and N is the number of cycles.

3. Piezoelectric sensor

PZT-5H is the most common engineering piezoelectric sensor and has the best piezoelectric ceramic material properties. In this work, the governing equation between the piezoelectric (PZT) effect and displacement is used for the finite element simulation of PZT-5H.

3.1 Piezoelectric orthotropic material

The PZT effect is a physical phenomenon where a solid sur-

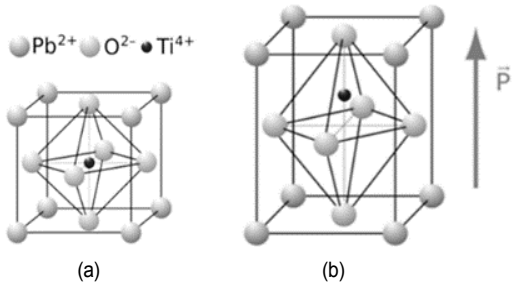

Fig. 3. (a) Perovskite structure above the Curie point; (b) perovskite unit cell showing the off-centered titanium ion [21].

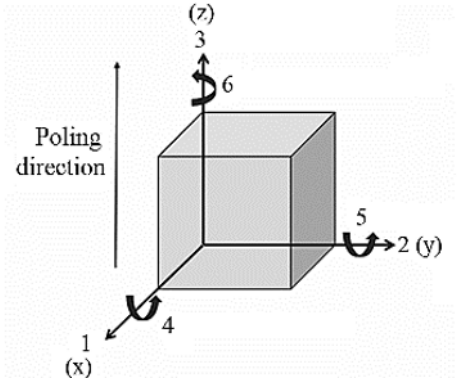

Fig. 4. Orthogonal coordinate system and poling direction [22].

face generates electric polarization when pressure is applied to the solid. Fig. 3(a) shows a Perovskite structure where 11 of the 32 crystal symmetries are at a central symmetry and 20 out of 21 non-central crystal symmetry shows piezoelectricity. A PZT sensor is a representative of multi-crystal piezoelectricity, which is generated by the poling process, as shown in Fig. 3(b). When a force is applied to non-central crystal symmetry, it transforms to electric dipole and generates the PZT effect of the sensor function. Conversely, when an electric voltage is applied, ions move to the opposite pole and can extend or shrink the crystal, which is called the inverse PZT effect of the actuator function [1]. Since dipoles have a directional property, adopting an orthogonal coordinate system is required to explain the behavior of the piezoelectric materials. Fig. 4 illustrates an orthogonal coordinate system (1-2-3) based on the poling direction. The material constants can have two subscripts; the first one represents the direction of the electric field while the second represents the direction of mechanical deformation. For example, in the crystal structure, the coupling coefficient d_{31} explains how much strain occurs in the x direction when the electric field is imposed in the z direction. It is critical to align the material coordinate system and principal directions in the simulation [2].

3.2 Piezoelectric constitutive formulas

The characteristics of PZT and inverse PZT effects can be represented using electric and mechanical parameters in orthogonal coordinates. The piezoelectric coefficient matrix is obtained as Eq. (4) [23]. The PZT coefficient matrix is either the polarization generated per unit of mechanical stress applied to PZT material or the mechanical strain experienced by PZT material per unit of an applied electric field.

$$d_{mij}^{\varphi}=\begin{bmatrix} d_{111} & d_{122} & d_{133} & d_{112} & d_{113} & d_{123} \\ d_{211} & d_{222} & d_{233} & d_{212} & d_{213} & d_{223} \\ d_{311} & d_{322} & d_{333} & d_{312} & d_{313} & d_{323} \end{bmatrix}. \tag{4}$$

The first index on these coefficients refers to the component of electric displacement, while the last pair of indices refer to the component of mechanical stress or strain. Because the strain induced in PZT material by an applied electric field is the product of the value for the electric field and the corresponding component in the d matrix, d is an important indicator of material suitability for a PZT actuator. The triple index notation can be converted easily to the required double index notation using a conventional method.

PZT material responds to an electric potential gradient by straining, while stress causes an electric potential gradient in the material. Eq. (5) denotes the strain tensor generated by the electric potential gradient and mechanical stress and Eq. (6) shows the electric displacement vector generated by mechanical strain and electric potential gradient [2, 23]. The strain matrix represents the actuator function of PZT to produce mechanical motion, while the electric displacement matrix represents the sensor function of PZT.

$$\varepsilon_{ij}=d_{mij}^{\varphi}E_m+S_{ijkl}^{E}\sigma_{kl} \tag{5}$$

$$q_i=d_{ijk}^{\varphi}\sigma_{jk}+D_{ij}^{\varphi(\sigma)}E_j\,. \tag{6}$$

In Eqs. (5) and (6), d is the PZT strain coefficient matrix, E is the electrical potential gradient vector, S is the elastic compliance for stress and σ is the mechanical stress tensor. The superscripts E, φ, or σ indicate that the property is defined at zero electrical gradient, zero electrical displacement, and zero stress, respectively.

3.3 Piezoelectric material properties

The PZT actuator and sensor used in this research is PZT-5H, whose PZT coefficient matrix at 25 °C is given in the following equation:

$$d_{mij}^{\varphi}=\begin{bmatrix} 0 & 0 & 0 & 741 & 0 & 0 \\ 0 & 0 & 0 & 0 & 0 & 741 \\ -274 & 593 & -274 & 0 & 0 & 0 \end{bmatrix}10^{-12}\,m/V\,. \tag{7}$$

The mechanical characteristics of PZT-5H are shown in Table 1 [29-31].

Table 1. Material properties of PZT-5H [29-31].

Parameter	Value
Radius (m)	0.0035
Thickness (m)	0.0002
Density (kg/m²)	7800
Young's modulus E_1 (GPa)	60.61
Young's modulus E_2 (GPa)	60.61
Young's modulus E_3 (GPa)	48.31
Poisson's ratio ν_{12}	0.512
Poisson's ratio ν_{13}	0.408
Poisson's ratio ν_{23}	0.289
Shear modulus G_{12} (GPa)	23.0
Shear modulus G_{13} (GPa)	23.0
Shear modulus G_{23} (GPa)	23.5

4. Finite element model development

Here, we present an effective model to simulate the effect of a PZT actuator and sensor that can capture Lamb wave signals. To perform a finite element simulation, the commercial software Abaqus was used. Implicit time integration of a nonlinear dynamic analysis was used to simulate the wave propagation.

4.1 Element size

Table 2 shows the material properties of the Aluminum 2024-T3 plate used in both the simulation and experiment. It is imperative to select the maximum element size for the simulation to avoid aliasing between the shortest wave and the transverse wave propagating slowly [24].

To obtain the maximum element size, we must first calculate the speed of the transverse wave and the shortest wave length. The transverse wave speed of the Al 2024-T3 plate is given in Eq. (8), and the shortest wave length is calculated using Eq. (9) considering a 160 KHz frequency. By using these two equations, the allowable largest element size is calculated in Eq. (10) [32, 33]. By considering the size of the PZT sensors, the maximum element size is determined to be 1.0 mm.

$$C_T = \sqrt{\frac{G}{\rho}} = \sqrt{\frac{\mu}{\rho}} = \sqrt{\frac{E}{2\rho(1+\upsilon)}} \tag{8}$$

$$\lambda_{min} = \frac{C_T}{f} \tag{9}$$

$$L_{max} \le \frac{\lambda_{min}}{10}. \tag{10}$$

In Eqs. (8)-(10), C_T is the transverse wave speed, G is the shear modulus, ρ is the density, υ is the Poisson's ratio, μ is Lamb constants, E is Young's modulus, f is the Lamb wave frequency, and L is the element size.

Table 2. Material properties of aluminum 2024-T3.

Thickness (m)	0.002
Density (kg/m²)	2780
Young's modulus (GPa)	72.00
Poisson's ratio	0.33

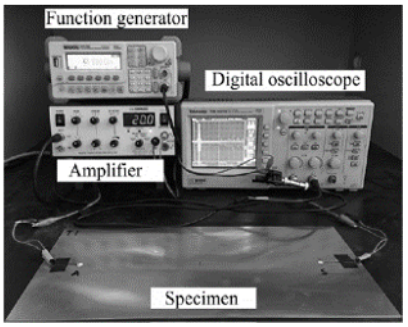

(a)

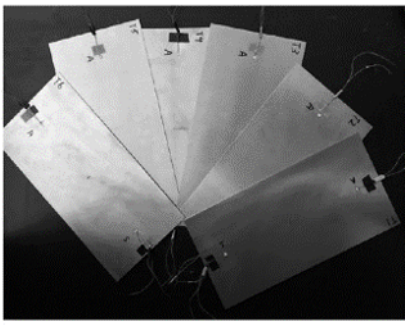

(b)

Fig. 5. (a) Experimental setup; (b) aluminum 2024-T3 specimen with PZT-5 sensors in a pitch-catch configuration.

4.2 Time step of analysis

Determining the appropriate time step of the time integration is essential to guarantee the accuracy of the nonlinear dynamic analysis. In general, accuracy is improved with a small-time step with a high computational cost. Conversely, the high frequency response will be inaccurately simulated if the time step is too large [25]. The longitudinal wave speed is first calculated using Eq. (11) and the time step is calculated based on Eq. (12). In addition, to be able to detect one wavelet within a time step, element sizes must also be calculated based on longitudinal wave speed when meshing a model. In this work, a time step of 0.2 μs is used considering the longitudinal speed of 5051 m/s and the element size of 0.1 mm for the 2 mm thickness Al 2024-T3 plate.

$$C_L = \sqrt{\frac{E}{\rho}} \tag{11}$$

$$\Delta t = \frac{L}{C_L}. \tag{12}$$

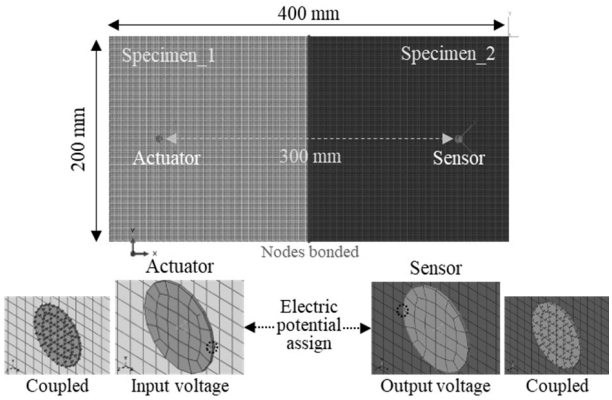

Fig. 6. Schematic and finite element model constraints of a specimen model with a 90° incident angle.

In Eqs. (11) and (12), C_L is the longitudinal wave speed, E is Young's modulus, ρ is the density, Δt is the simulation time step, and L is the element size.

4.3 Finite element model

In this work, a finite element model is constructed considering the experimental setup in Ref. [26] shown in Fig. 5: a Lamb wave testing experiment on aluminum 2024-T3 plates with cracks of different sizes. Our finite element model consists of aluminum 2024-T3 plates with PZT-5H actuator/sensor. Two half plates are partially connected using a 'tie' constraint to represent cracks with various sizes. To provide the Lamb wave signals in the form of the electric potential to the PZT actuator/sensor, all nodes in a PZT actuator/sensor are connected with a reference node via linear constraint equations. Fig. 6 shows the finite element model of the plate and PZT actuator/sensor. In the actuator, the electric potential is assigned in the form of tone-bust signals, which is converted into strain, as shown in Eq. (5). After the generated wave is propagated through the plate, the sensor converts the strain into the output voltage using Eq. (6).

4.4 Results and validation

The first step in the simulation is to calibrate the simulation parameters and validate the simulation prediction against experimental measurements [5, 27]. The Lamb wave signal can be obtained in the pitch-catch configuration. The amplitude of the received signal will be reduced if the crack size increases in the pitch-catch method. The forward scattered wave takes detours to the sensors once it encounters a crack. Thus, the time of arrival of the received signal will be delayed as the crack size increases. This feature is the phase change of the signal, which means the time-of-flight (ToF) difference between undamaged signal and damaged signal. Also, the reflection of signal is related to the distance between the sensor and damage in such a way that the amplitude of reflected wave would decrease due to wave attenuation and dispersion with the increased distance where the damage is regarded as a new wave source. Such a phenomenon complicates effective damage identification based on wave scattering [34-36].

Table 3. Lamb wave characteristics introduced by the change of crack size with experimental and simulation results.

	Crack lengths (mm)	Phase change	Normalized amplitude
Experimental	0	0	1
	8	0.1	0.9200
	20	0.3	0.7962
	30	0.6	0.6669
Simulation	0	0	1
	8	0.2	0.9278
	20	0.3	0.7923
	30	0.6	0.6809

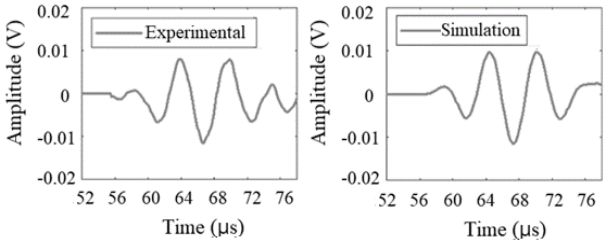

Fig. 7. Experimental and simulation Lamb wave data with an incident angle of 90° and 0 mm crack.

Among various types of waves, S_0 mode is known to be sensitive to cracks [27]; therefore, we also utilized S_0 mode for analyzing signal characteristics. First, signals on the no-crack plate are used for calibrating the simulation model. When the distance between the actuator and sensor is 300 mm, the arrival time of an S_0 mode Lamb wave with 160 kHz is 56.3 μs. Fig. 7 shows that the signals from the simulation and experiment arrived at the same time. The damping coefficient proportional to stiffness is adjusted so that the amplitudes in the simulation and experiment match each other. Table 3 shows the change in phase angle and the normalized amplitude when the incident angle is 90°. The crack signal amplitudes are normalized with the no-crack signal amplitude. We found that as the crack size increases, the normalized amplitude decreases, but the phase angle increases. Based on the above results, it is possible to develop a quantitative model because the signal is clearly different depending on the size of the crack. A quantitative model based on the normalized amplitude and phase change can be used to estimate the crack size.

5. Incident angle crack model

It is unrealistic that a crack will grow in a perpendicular direction to the actuator-sensor line. Therefore, to study the effect of orientation of the crack to the sensor signals, cracks of various angles were simulated using a finite element analyses.

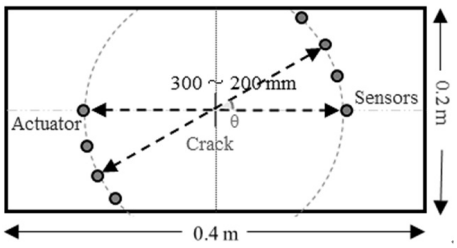

Fig. 8. First finite element model of the simulation with variable incident angles with crack sizes and sensor locations.

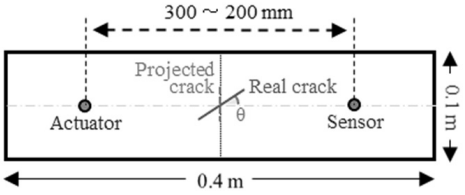

Fig. 9. Second finite element model of the simulation with variable incident angles with crack sizes and sensor locations.

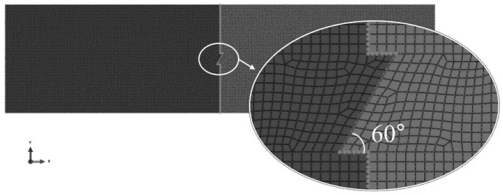

Fig. 10. The shape of the element around the incident angle crack of 60° with a size of 10 mm in the second finite element model.

5.1 Incident angle with various sensor distance

In this work, the incident angles were set to 45°, 60°, 75°, and 90° while the crack size varied between 10 mm and 30 mm in an increment of 5 mm. To find the effect of distance between the sensor and crack, the distance also varied to 300 mm, 250 mm, and 200 mm. Two crack models were used to investigate the effect of element orientation on signal propagation. The first model is the one validated in Sec. 4, as shown in Fig. 8. In this model, the crack location and orientation are fixed. Four sensors and actuators are located in a circular pattern at 15° intervals so that the aforementioned angles can be realized. The radius of the circular pattern is also changed to examine the effect of the sensor-actuator distance. However, the wave propagation in different angles may be affected by the element direction. In the second model, to minimize the effect of element orientation, the direction of the sensor and actuator are fixed, while the orientation of the crack is changed, as shown in Fig. 9. In this model, the projected crack size normal to the sensor-actuator line is first determined. The real crack size is then calculated using the trigonometric relationship. In addition, to reduce the computational cost, the width of the plate is reduced by a half. As shown in Fig. 10, the element near the crack is rectangular-shaped, but most other regions have a 1 mm square-shaped element.

Table 4. Signal characteristic data for a sensor distance of 250 mm and an incident angle of 75° in the simulation of the first finite element model.

Incident angle	Crack lengths (mm)	Phase change	Normalized amplitude
75°	0	0	1
	10	0.38	0.8781
	15	0.43	0.8152
	20	0.55	0.7753
	25	0.70	0.7208
	30	0.83	0.6598

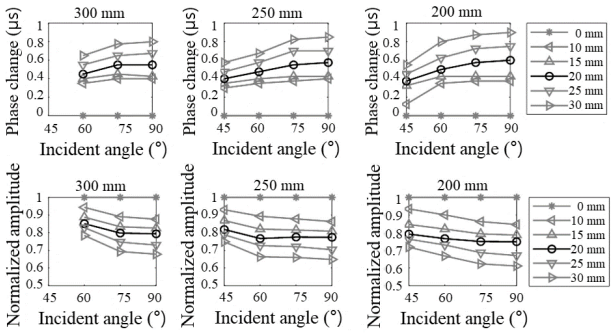

Fig. 11. Influence of variable incident angle with crack sizes and sensor locations on the first finite element model.

5.2 Result and discussion

This section presents the results from the two models at different orientations. For both models, the arrival times of the S_0 mode with a distance of 250 mm and 200 mm were 46.9 μs and 37.5 μs, respectively. All results were normalized by the no-crack case. Table 4 summarizes the effect of crack size on the change of phase angle and the normalized amplitude when the incident angle is 75° using the first model. Fig. 11 summarizes the change of phase angle and the normalized amplitude for different crack sizes, distances, and incident angles. The summarized results of the second model are shown in Table 5 and Fig. 12.

For the first model, we found that the phase angle and amplitude converge to the no-crack case as the incident angle decreases. This is because the sensitivity to the crack is reduced as the angle decreases. The characteristics of the Lamb wave become clear as the distance between the actuator and sensor decreases, and the effect of crack size increases as the incident angle increases. For the second model, there is not much variation in the phase angle as the incident angle decreases. This is likely due to the phase change being smaller than the first model as it minimized the influence of the mesh over the first model in which waves propagated along the diagonal of the square elements. It can also be seen that the normalized amplitude changes minimally when the incident angle decreases. This is because the second model does not change signals much because the projected crack size remains constant even if the real crack size increases as the incident angle

Table 5. Signal characteristic data for a sensor distance of 250 mm and an incident angle of 75° in the simulation of the second finite element model.

Incident angle	Crack lengths (mm)	Phase change	Normalized amplitude
75°	0	0	1
	10	0.20	0.8544
	20	0.38	0.7341
	30	0.65	0.5701

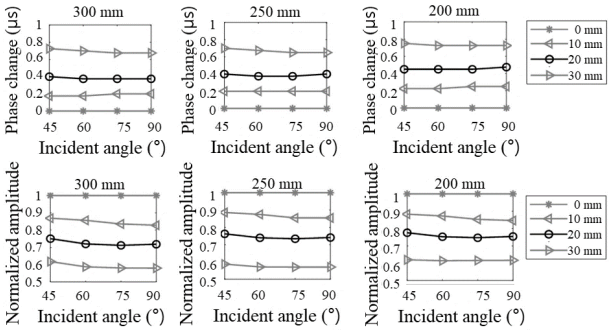

Fig. 12. Influence of variable incident angle with crack sizes and sensor locations on second finite element model.

decreases. The mesh influence and sensor direction effect will be investigated with additional experiments and finite element models in future studies.

6. Conclusions

This research presents a method of simulating Lamb wave propagation over a cracked plate. A PZT actuator and sensor are modeled using a finite element to effectively represent the behavior of a Lamb wave. The simulation utilized S_0 mode waves, which are sensitive to crack damage on an aluminum plate. The simulation parameters were calibrated using the experimental data over a no-crack plate. Based on simulations with various incident angles and the distances between the PZT actuator and sensor, the phase angle and amplitude changes were analyzed to yield the following conclusions.

1) We constructed an FE model of a PZT actuator and sensor. This FE model was verified through experiments on the phase change and normalized amplitude according to the crack size in the crack perpendicular to the sensor. This model can be used to detect various inclined cracks in a structure.

2) Based on the FE simulation results, we confirmed that the signal characteristics due to cracks clearly show a change in signal characteristics as the incident angle increases. As the incident angle increases, the amplitude changes increase.

3) The size and the incident angle of the crack significantly affect the change in signal characteristics and the effect increases as the incident angle increases. In addition, as the distance between the actuator and sensor decreases, the difference in signals becomes clearer.

In this study, we confirmed that the incident angle, crack size and distance affect the characteristics of Lamb wave signals. This work requires further validation using additional experiments. Developing a reliable model with parameters that can influence the signal characteristic is required, which can eventually lead to more accurate prediction. Lastly, cracks in real applications are not straight; therefore, it is necessary to investigate the signal characteristics as a function of crack shape. For that purpose, an adequate method of meshing the cracked plate must be identified with further experimental validation.

Acknowledgments

This research was supported by the Ministry of Trade, Industry and Energy (MOTIE) and Korea Institute for Advancement of Technology (KIAT) through the Project of Global Human Resources Cultivation for Innovative Growth (Project No.: P0008751).

Nomenclature

$S(t)$: SIN function
$W(t)$: Hanning window function
$y(t)$: Tone burst signal
d_{mij}^{φ} : Piezoelectric coefficient matrix
ε_{ij} : Strain vector
q_m : Electric displacement matrix
C_T : Transverse wave speed
λ_{min} : Shortest wave length
L : Element size
C_L : Longitudinal wave speed
Δt : Time step of analysis
f : Center frequency of lamb wave
t : Total signal time of lamb wave

References

[1] V. Giurgiutiu, Tuned Lamb wave excitation and detection with piezoelectric wafer active sensors for structural health monitoring, *Journal of Intelligent Material Systems and Structures*, 16 (4) (2006) 291-305.

[2] S. Lin, T. Ito, K. Kawashima, M. Okade and H. Nagamizo, Sizing of axial defects in pipes with FEM simulation of wave propagation and wavelet transformation, *IEEE Ultrasonics Symposium* (1998) 877-880.

[3] X. Zhu, *Piezoelectric Ceramic Materials: Processing, Properties, Characterization, and Applications*, Nova Science Publishers, New York, UK (2010).

[4] V. Giurgiutiu, *Structural Health Monitoring: with Piezoelectric Wafer Active Sensors*, 2nd Ed., Academic Press, New York (2014).

[5] J.-B. Ihn and F.-K. Chang, Detection and monitoring of hidden fatigue crack growth using a built-in piezoelectric sensor/actuator network: II. Validation using riveted joints and repair patches, *Smart Materials and Structures*, 13 (3) (2004) 621-630.

[6] Y. Lu, Z. Su and C. Yang, Quantitative assessment of through-thickness crack size based on Lamb wave scattering in aluminium plates, *NDT & E. Int.,* 41 (1) (2008) 59-68.

[7] J.-B. Ihn and F.-K. Chang, Detection and monitoring of hidden fa-

tigue crack growth using a built-in piezoelectric sensor/actuator network: I, Diagn, *Smart Materials and Structures*, 13 (3) (2004) 609.
[8] X. P. Qing, S. Beard, S. B. Banerjee, M. M. Salama and F-K. Chang, Development of a real-time active pipeline integrity detection system, *Smart Materials and Structures*, 18 (11) (2009) 115010.
[9] J. E. Michaels and T. E. Michaels, Detection of structural damage from the local temporal coherence of diffuse ultrasonic signals, *IEEE Transactions on Ultrasonics, Ferroelectrics, and Frequency Control,* 52 (10) (2005) 1769-1782.
[10] Y-S. Roh, Built-in diagnostics for identifying an anomaly in plates using wave scattering, *Doctoral Dissertation*, Stanford University, California (1999).
[11] C. Wang and F. Chang, Built-in diagnostics for impact damage identification of composite structures, *Proceedings of the 2nd International Workshop on Structural Health Monitoring* (1999) 8-10.
[12] J. Y. Zhou, L. Xiao, W. Z. Qu and Y. Lu, Nonlinear Lamb wave based DORT method for detection of fatigue cracks, *NDT & E International*, 92 (2017) 22-29.
[13] J. P. Andrews, Lamb wave propagation in varying thermal environments, *Master's Thesis*, Air Force Institute of Technology, Ohio, USA (2012).
[14] Z. Youxuan, Generation mechanism of nonlinear ultrasonic Lamb waves in thin plates with randomly distributed microcracks, *Ultrasonics*, 79 (2017) 60-67.
[15] H. Lamb, On waves in an elastic plate, *Proceedings of the Royal Society of London*, 93 (648) (1917) 114-128.
[16] G. R. Kirikera, V. Shinde, M. J. Schulz, A. Ghoshal, M. Sundaresan and R. Allemang, Damage localisation in composite and metallic structures using a structural neural system and simulated acoustic emissions, *Mechanical Systems and Signal Processing*, 21 (1) (2007) 280-297.
[17] P. Kudela, W. Ostachowicz and A. Zak, Damage detection in composite plates with embedded PZT transducers, *Mechanical Systems and Signal Processing*, 22 (6) (2008) 1327-1335.
[18] L. Yu and V. Giurgiutiu, In-situ optimized PWAS phased arrays for Lamb wave structural health monitoring, *Journal of Mechanics of Materials and Structures*, 2 (3) (2007) 459-487.
[19] C. Zhou, Z. Su and L. Cheng, Quantitative evaluation of orientation-specific damage using elastic waves and probability-based diagnostic imaging, *Mechanical Systems and Signal Processing*, 25 (6) (2011) 2135-2156.
[20] P. Kudela, M. Radzieński and W. Ostachowicz, Identification of cracks in thin-walled structures by means of wavenumber filtering, *Mechanical Systems and Signal Processing*, 50 (2015) 456-466.
[21] LibreTexts Chemistry, *6.3: Crystal Structure*, LibreTexts Chemistry, https://chem.libretexts.org/Courses/Douglas_College/DC%3A_Chem_2330_(O'Connor)/6%3A_Solids/6.3%3A_Crystal_Structure.
[22] S. Priya, H-C. Song, Y. Zhou, R. Varghese, A. Chopra, S-G. Kim, I. Kanno, L. Wu, D.-S. Ha, J. Ryu and R. G. Polcawich, A review on piezoelectric energy harvesting: materials, methods, and circuits, *Energy Harvesting and Systems,* 4 (1) (2016) 0028.
[23] T. Ikeda, *Fundamentals of Piezoelectricity*, Oxford University Press, New York, USA (1990).
[24] D. Alleyne and P. Cawley, A two-dimensional Fourier transform method for the measurement of propagating multimode signals, *Journal of the Acoustical Society of America*, 89 (3) (1991) 1159-1168.
[25] F. Moser, L. J. Jacobs and J. Qu, Modeling elastic wave propagation in waveguides with the finite element method, *NDT&E International*, 32 (4) (1999) 225-234.
[26] F. Sun, N. Wang, J. He, X. Guan and J. Yang, Lamb wave damage quantification using GA-based LS-SVM, *Materials*, 10 (6) (2017) 648.
[27] E. Le, M. Castaings and B. Hosten, The interaction of the S0 lamb mode with vertical cracks in an aluminum plate, *Journal of Ultrasonics*, 40 (1-8) (2002) 187-192.
[28] E. Le, M. Castaings and B. Hosten, The interaction of the S0 lamb mode with vertical cracks in an aluminum plate, *Journal of Ultrasonics*, 40 (1-8) (2002) 187-192.
[29] eFunda, Inc., *Lead Zirconate Titanate (PZT-5H)*, eFunda, Inc., https://www.efunda.com/materials/piezo/material_data/matdata_output.cfm?Material_ID=PZT-5H.
[30] E. Heinonen, J. Juuti and S. Leppavuori, Characterization and modelling of 3D piezoelectric ceramic structures with ATILA software, *Journal of European Ceramic Society*, 25 (12) (2005) 2467-2470.
[31] ANSI/IEEE Std 176-1987, *IEEE Standard on Piezoelectricity*, IEEE (1988).
[32] M. Gresil, V. Giurgiutiu, V. Shen and B. Poddar, Guidelines for using the finite element method for modeling guided lamb wave propagation in SHM processes, *6th European Workshop on Structural Health Monitoring*, Dresden, Germany (2012) 3-6.
[33] T. Wang, Finite element modelling and simulation of guided wave propagation in steel structural members, *Ph.D. Thesis*, University of Western Sydney, Sydney, Australia (2014).
[34] O. Diligent, T. Grahn, A. Boström, P. Cawley and M. J. S. Lowe, The low-frequency reflection and scattering of the S0 Lamb mode from a circular through-thickness hole in a plate: finite element, analytical and experimental studies, *The Journal of the Acoustical Society of America,* 112 (6) (2002) 2589-601.
[35] R. P. Dalton, P. Cawley and M. J. S. Lowe, The potential of guided waves for monitoring large areas of metallic aircraft fuselage structure, *Journal of Nondestructive Evaluation*, 20 (2001) 29-46.
[36] Y. Lu, L. Ye, S. Z. Su and N. Huang, Quantitative evaluation of crack orientation in aluminium plates based on Lamb waves, *Smart Materials and Structures*, 16 (5) (2007) 1907-1914.

Seyeon Kim received her B.E. degree in the Department of Mechanical Engineering in 2019 from Keimyung University, Daegu, South Korea. She is currently pursuing her Ph.D. in the Department of Mechanical Engineering at the same university. Her research interests include reliability-based design optimization and nuclear technology.

Nam-Ho Kim is currently a Professor of Mechanical and Aerospace Engineering at the University of Florida. He graduated with a Ph.D. in the Department of Mechanical Engineering from the University of Iowa in 1999 and worked at the Center for Computer-Aided Design as a post-doctoral associate until 2001. His research area is structural design optimization, design sensitivity analysis, design under uncertainty, structural health monitoring, nonlinear structural mechanics, and structural-acoustics. He has published three books and more than one hundred refereed journal and conference papers in the above areas.

Sanghoon Lee is currently an Associate Professor of Mechanical Engineering at Keimyung University, Daegu, South Korea. He graduated with a Ph.D. in the Department of Mechanical Engineering from the Korea Advanced Institute of Science and Technology in 2006 and worked at the Korea Atomic Energy Research Institute as a Senior Researcher until 2015. His research areas are design optimization, design under uncertainty, and waste package design and safety evaluation. He has been published in more than 60 journals and conference papers in the above areas.